Vol 15 No 12, December 2006
1009-1963/2006/15(12)/2984-05

Chinese Physics

© 2006 Chin. Phys. Soc.
and IOP Publishing Ltd

Different localized states of travelling-wave convection in a rectangular container *

Li Guo-Dong(李国栋)[a)†] and Huang Yong-Nian(黄永念)[b)]

[a)] *Institute of Water Resources and Hydro-electric Engineering, Xi'an University of Technology, Xi'an* 710048, *China*

[b)] *State Key Laboratory for Studies of Turbulence and Complex Systems, Peking University, Beijing* 100871, *China*

(Received 1 September 2005; revised manuscript received 13 July 2006)

We have performed numerical simulations of localized travelling-wave convection in a binary fluid mixture heated from below in a long rectangular container. Calculations are carried out in a vertical cross section of the rolls perpendicular to their axes. For a negative enough separation ratio, two types of quite different confined states were documented by applying different control processes. One branch of localized travelling waves survives only in a very narrow band within subcritical regime, while another branch straddles the onset of convection existing both in subcritical and supercritical regions. We elucidated that concentration field and its current are key to understand how confined convection is sustained when conductive state is absolutely unstable. The weak structures in the conducting region are demonstrated too.

Keywords: binary fluid mixture, travelling-wave convection, localized states

PACC: 4754, 4752, 4725Q, 4735

Pattern formation and spatiotemporal dynamics in a variety of nonequilibrium systems have attracted a great deal of research activities in recent decades.[1−4] Of particular interest is the convection in a thin, horizontal layer of a binary fluid mixture heated from below, in which complex time-dependent behaviours present even very close to the onset of the initial instability.[5,6] The most fascinating phenomenon observed in binary fluid convection is the localization of travelling wave (TW): that is, convection rolls moving in a direction perpendicular to their axes do not fill the entire experimental cell but a part of it, and in that restricted space convecting regions coexist stably with nonconvecting regions.[7,8] Most of the localized travelling waves (LTWs) were found in the subcritical region below the bifurcation threshold for the onset of convection,[9−11] where both convective and conductive states are stable. For weak Soret coupling, e.g. $\Psi = -0.08$, experimental LTWs were also observed to exist above the convective threshold in convectively unstable regime.[12]

In this paper, following numerical simulations of two-dimensional Boussinesq field equations in a rectangular container under experimental boundary conditions, we found that a localized state can straddle the onset of convection over a broad band of Rayleigh numbers for a strongly negative Soret coupling $\Psi = -0.25$. The LTW states that exist only at subcritical region below the convection threshold were documented too at this separation ratio Ψ. In both cases, the LTWs settle on one side wall of the container, but with different front structures. A feedback mechanism between the LTW field and a large-scale mean lateral concentration current loop leads to a concentration redistribution within the LTW. Different concentration redistributions under leading-edge and trailing-edge fronts can explain the observed dynamical behaviours.

We consider here the idealized situation of planar flow in a vertical cross section through the convection rolls perpendicular to their axes. Based on the Oberbeck–Boussinesq approximation, the nondimensional balance equations for mass, momentum, heat, and concentration of this system are given as[13,14]

$$\nabla \cdot \boldsymbol{u} = 0, \tag{1}$$

$$(\partial_t + \boldsymbol{u} \cdot \nabla)\boldsymbol{u} = \sigma\nabla^2\boldsymbol{u} - \nabla p + R \cdot \sigma[(1+\Psi)\delta T + \delta\eta]\mathbf{e}_z, \tag{2}$$

$$(\partial_t + \boldsymbol{u} \cdot \nabla)\delta T = \nabla^2 \delta T, \tag{3}$$

*Project Supported by the Scientific Research Foundation for the Returned Overseas Chinese Scholars, Ministry of Education of China, and the Special Foundation for State Major Basic Research Program of China (Grant No G20000773).

†E-mail: gdli2002@pkuaa.edu.cn

$$(\partial_t + \boldsymbol{u}\cdot\nabla)\delta\eta = L\nabla^2\delta\eta - \Psi\nabla^2\delta T, \qquad (4)$$

where α is the thermal expansion coefficient, β is the solute expansion coefficient, and k is the thermal diffusivity. Here the lengths are scaled by the height d of the layer, time by the vertical thermal diffusion time $t_v = d^2/k$ and the velocity field $\boldsymbol{u} = (u, w)$ by k/d. We introduce the combined field $\delta\eta = \delta C - \Psi\delta T$ for convenience, since the term $-L\nabla\delta\eta$ represents the diffusive current of concentration. The deviations δT of temperature and δC of concentration from their average values are scaled by the temperature difference ΔT across the layer and $(\alpha/\beta)\Delta T$ respectively. In our simulations, Lewis number $L = 0.01$, and Prandtl number $\sigma = 10$ are typical for room-temperature ethanol-water mixtures. We applied laterally no slip, insulating and impermeable boundary conditions at $x = 0$ and Γ with aspect ratio $\Gamma = 14$. Horizontal boundaries at top and bottom $z = 0$ and 1 also are realistic, i.e. no slip, perfectly heat conducting and impermeable. Our control parameter $r = R/R_c^0$ measuring the thermal driving is the Rayleigh number R reduced by the critical one $R_c^0 = 1708$ for the onset of convection in a pure fluid.

The calculations began by raising r a few percent above the onset $r_{osc} = 1.363$ with round-off errors serving as small random perturbation to the system. As observed previously in experiments,[15] counterpropagating TW that occupied the entire rectangle during the early stages eventually evolved into confined domains of primarily left-going TW in the left half of the rectangular cell. If r is held above r_{osc}, this confined convection expands to fill the entire cell with slow TW. However, this can be avoided by reducing r during this phase. If r is dropped to within a narrow band below the threshold point, then the confined state can be maintained as shown in Fig.1(a).

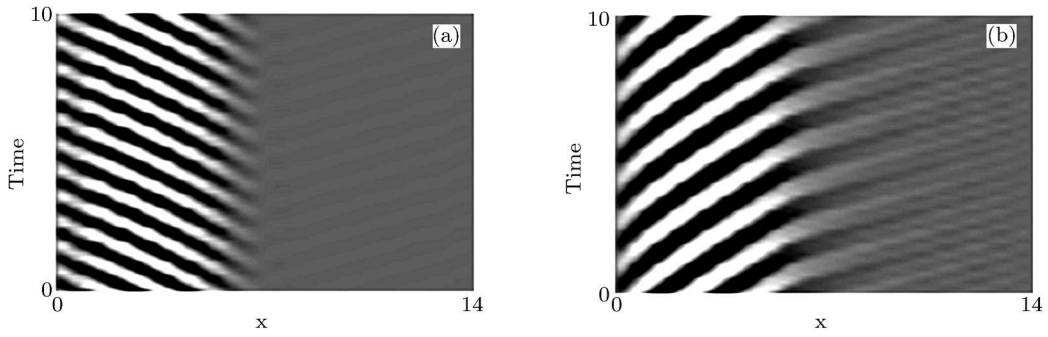


Fig.1. Gray-scale spatiotemporal plots for two apparently different types of localized travelling waves at the same $r = 1.35$. (a) Fast confined state with trailing-edge front and (b) slow confined state with leading -edge front. The light (dark) area corresponds to up-(down-) flow of the convection rolls.

Its leading-edge (defined as the boundary of confined region from which rolls annihilate, as opposed to the opposite trailing-edge where convective rolls originate) coincides with the left end wall of the cell, and the rolls in this confined state exhibit a relatively high oscillation frequency $\omega = 7.0\,(\kappa/d^2)$. In another run, we first applied laterally periodic boundary conditions at $x = 0$ and Γ; when nonlinearity set in, the boundary conditions were changed to experimental wall boundary conditions as described above. In this way, another type of localized states is obtained. An example is presented in Fig.1(b) with a relatively low oscillation frequency $\omega = 4.2\,(\kappa/d^2)$. Since this type of LTWs travels much slower than the former (at the same r), we refer to such states as slow confined states (SCSs), while the former is referred to as fast confined states (FCSs). One should also notice that, for SCSs, it is their trailing-edges that touch the cell wall.

As illustrated in Fig.2, the SCSs are not only stable in the hysteric region but also stable up to a reduced Rayleigh number $r = 1.42$ far beyond the convection onset, with a stable r interval about the order of $O(10^{-1})$.

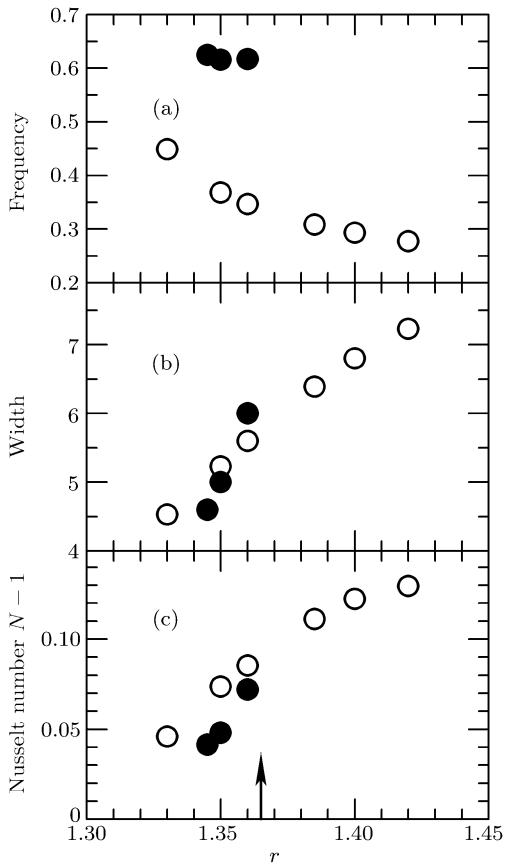


Fig.2. Positions and stable regions of the two types of LTW states. (a) The oscillation frequency, (b) the width, and (c) Nusselt number $N-1$ as functions of the reduced Rayleigh number r. The convection is triggered at $r_{\rm osc} = 1.363$, with a Hopf frequency $\omega_{\rm H} = 11(\kappa/d^2)$. Solid circle branch with higher frequency will be referred to as fast confined state (FCS), and open circle branch with smaller frequency will be referred to as slow confined state (SCS).

For the FCS branch, this r interval is only of the order of $O(10^{-2})$. In addition to oscillation frequency, Fig.2 also shows the width of LTWs and convection contribution $N-1$ to the Nusselt number, where N is defined as the ratio of the effective thermal conductivity of the fluid layer to that due to the thermal conduction alone. Both the width and Nusselt number increase as r is increased, and they are roughly the same for both types of confined states in multi-stable region. The oscillation frequency of SCSs is observed to decrease smoothly as r is increased. If r is increased beyond the limit of stable band, the leading edge of SCSs will continuously expand to reach the opposite wall until the entire cell is filled with large amplitude convecting rolls. During this transition, the Nusselt number $N-1$ has a sharp increase, while the change of oscillation frequency from LTW state to extended TW state is very smooth. If r is increased above the stable regime of FCSs, the front (sharp boundary region that separates the conducting and convecting dynamical states) is no longer stationary, but expands to fill the entire cell. Once the front reaches the opposite side of the cell, the oscillation frequency drops dramatically to a small value which is the same as that measured in the confined state of SCSs.

Figure 3(a) shows the lateral structures of the LTWs in the snapshots of vertical flow velocity w and concentration δC. There exists a phase shift between the concentration field and the velocity field in the centre part of the LTW. This shift leads to a strong time-averaged concentration current[13,16]

$$\langle J\rangle = <\boldsymbol{u}\delta C - L\nabla\delta\eta> \qquad (5)$$

that flows in the upper (lower) half of the layer parallel(anti-parallel) to the propagation direction of TW as depicted in Fig.3(b). At the fronts of the LTWs, the current bends over vertically since there is almost no concentration current in the conductive area, thus forming a large-scale circulation loop. On the other hand, the concentration difference between the conductive area and the centre part of LTWs will generate a lateral diffusive current $-L\partial_x\langle\delta C\rangle$ near the plates. While at the trailing front it strengthens slightly the primary concentration current circulation, and this diffusive effect counteracts the primary current and generates two small secondary countercirculating current loops at the leading front. As shown in Fig.3(c), the resulting concentration redistribution causes the mean convectively generated $\langle c\rangle = \langle\delta C - \delta C_{\rm con}\rangle$ profile to extend significantly further into the conducting region than the mean convective temperature field $\langle\theta\rangle = \langle\delta T - \delta T_{\rm con}\rangle$. Therefore, the convective contribution of the mean buoyancy force $\langle b\rangle = \langle c\rangle + \langle\theta\rangle$ is determined in the front region predominantly by the concentration field. The negative mean buoyancy force ahead of the leading front restabilizes the conduction here, which enables the SCSs to be stable in a very wide band of r even far beyond in the absolutely instable regime.[17] The increase of $\langle b\rangle$ out of the conductive state under the trailing front and its strong overshoot over the bulk can explain why the FCSs are much less stable than SCSs.

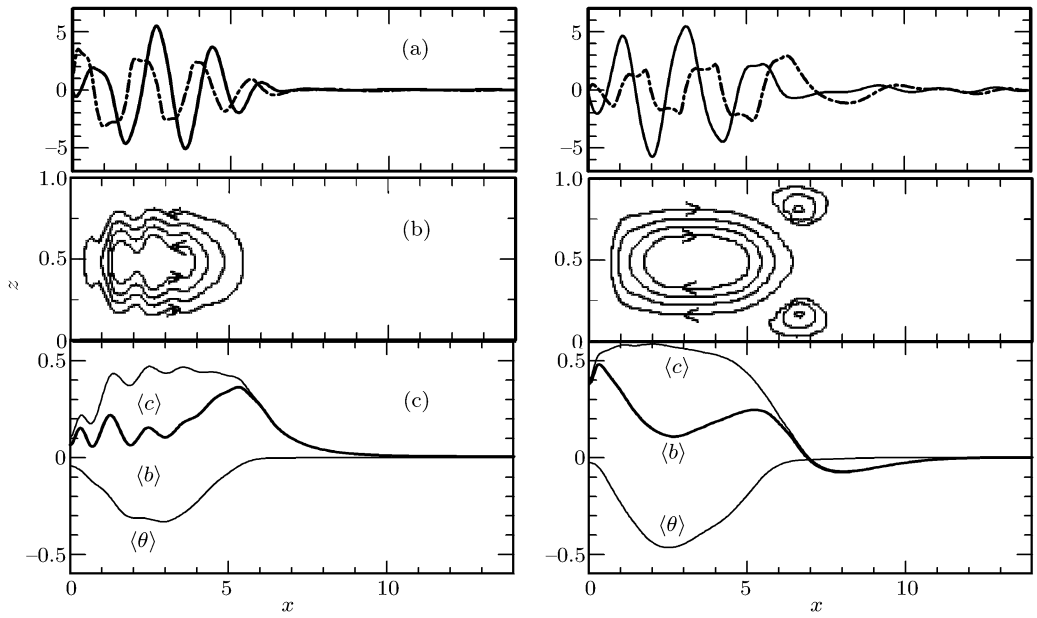


Fig.3. (a) Snapshots of lateral wave profiles at midheight, $z = 0.5$, of concentration C (dashed lines) and vertical velocity w (full lines). (b) Streamlines of time-averaged concentration current. (c) Time-averaged deviations from conductive state at $z = 0.25$ for concentration $\langle c\rangle$, temperature $\langle\theta\rangle$, and their sum $\langle b\rangle$ measuring the convective contribution to the mean buoyancy force. The left panel is for the fast confined state and the right panel is for the slow confined state at $r = 1.35$.

Since there are no experimental or measurement noises in the numerical simulations, it is possible to investigate the spatial structure of flow field in the conducting regions. Figure 4 shows the evolution of the midplane vertical velocity for the confined states at the convecting and conducting regions ($x/\Gamma = 0.2$ and 0.8). To our surprise, for FCS, although its amplitude in conducting region is only about 0.6% of the value in the convecting region, weak oscillation has the same frequency as that observed in the convecting region. The corresponding spatio-temporal structures is demonstrated in Fig.5(a). It is a right going wave which is originally counterpropagating partner of the left travelling-wave, but with faster phase velocity due to its smaller wave number. For the SCS, the weak oscillating amplitude is about 6% of that in convecting region, ten times larger than that in FCS. Apparently, it has two oscillation frequencies. The fundamental frequency is $\omega_0 = 11.38\,(\kappa/d^2)$, which corresponds to the frequency of the linear instability, while the second frequency is identical to that in convecting region. As shown in Fig.5(b), it also has quite different spatiotemporal structure from FCSs. When the amplitude of the underlying TW suddenly collapses at the leading-edge front, it is accompanied by an increase in TW wavelength and phase velocity. The increase in wavelength then leads to the rolls splitting, and simultaneously, a very weak counter propagating wave component coming from right wall can be seen taking part in the modulation.

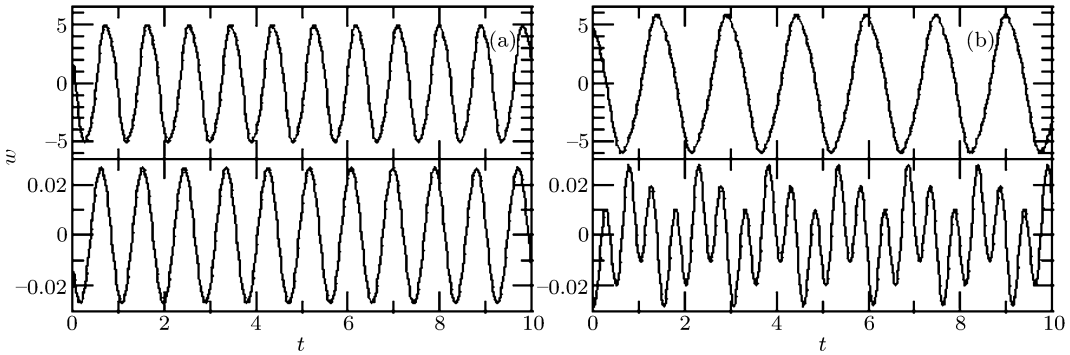


Fig.4. Time series of the vertical component of velocity at single spatial points taken from the middle height of the cell at $x/\Gamma = 0.2$ (top) and $x/\Gamma = 0.8$ (bottom) corresponding to the convection region and conductive region respectively. (a) Fast confined state and (b) slow confined state at $r = 1.35$.

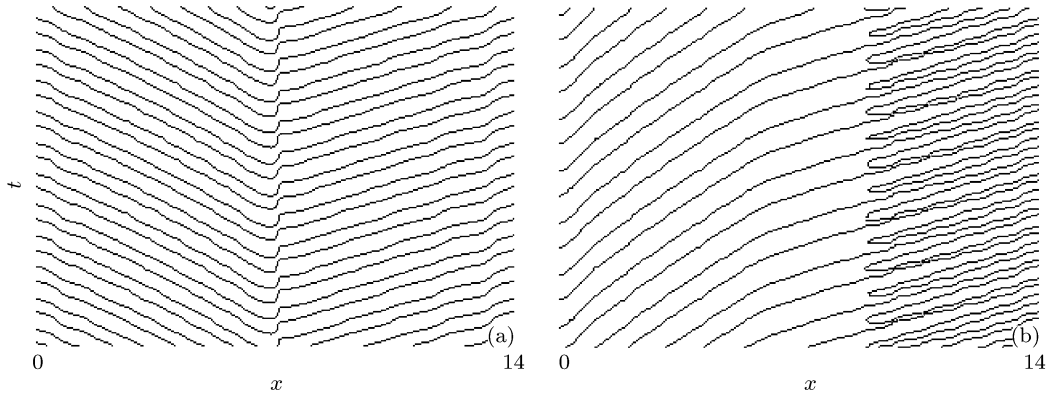


Fig.5. Space-time plots of flow patterns covering extremely weak structures in conducting area. Each line represents the trajectory of an individual roll boundary. (a) Fast confined state and (b) slow confined state at the same $r = 1.35$.

To summarize, we have found bistability between fast and slow confined states in a liquid mixture with strong Soret coupling $\Psi = -0.25$ in a rectangular container. Especially for SCS, its stable region even exceeds the limit of absolute instability.[17] Because one front of the LTW touches a wall, this provides us an opportunity to study the functions of different fronts. On the other hand, what role the weak structure plays in the LTW stability needs to be investigated further.

References

[1] Cross M C and Hohenberg P C 1993 *Rev. Mod. Phys.* **65** 851
[2] Jian Y J and E X Q 2004 *Chin. Phys.* **13** 1191
[3] Hashim I and Sarma T 2006 *J. Phys. Soc. Jap.* **75** 035001
[4] Chen X G and Song J B 2006 *Chin. Phys.* **15** 756
[5] Walden R W, Kolodner P, Passner A and Surko C M 1985 *Phys. Rev. Lett.* **55** 496
[6] Sullivan T S and Ahlers G 1988 *Phys. Rev.* A **38** 3143
[7] Moses E, Fineberg J and Steiberg V 1987 *Phys. Rev.* A **35** 2757
[8] Heinrichs R, Ahlers G and Cannell D S 1987 *Phys. Rev.* A **35** 2761
[9] Bensimon D, Kolodner P, Surko C M, Williams L and Croquwtte V 1990 *J. Fluid Mech.* **217** 441
[10] Kolodner P 1993 *Phys. Rev.* E **51** R4187
[11] Kolodner P 1991 *Phys. Rev.* A **43** 2878
[12] Niemela J J, Ahlers G and Cannel D 1990 *Phys. Rev. Lett.* **64** 1365
[13] Barten W, Lücke M, Kamps M and Schmitz R 1995 *Phys. Rev.* E **51** 5662
[14] Li G D and Huang Y N 2004 *Acta Phys. Sin.* **53** 3800 (in Chinese)
[15] Surko C M and Kolodner P 1987 *Phys. Rev. Lett.* **58** 2055
[16] Jung D and Lücke M 2002 *Phys. Rev. Lett.* **89** 054502
[17] Kaplan E and Steinberg V 1992 *Phys. Rev.* A **46** R2996